Plasmonic nano-antenna a-Si:H solar cell

Marcel Di Vece,[*] Yinghuan Kuang, Stephan N.F. van Duren, Jamie M. Charry, Lourens van Dijk, and Ruud E.I. Schropp

Debye Institute for Nanomaterials Science, Nanophotonics—Physics of Devices, Utrecht University, P.O. Box 80000, 3508 TA Utrecht, The Netherlands
[*]*m.divece@uu.nl*

Abstract: In this work the effects of plasmonics, nano-focusing, and orthogonalization of carrier and photon pathways are simultaneously explored by measuring the photocurrents in an elongated nano-scale solar cell with a silver nanoneedle inside. The silver nanoneedles formed the support of a conformally grown hydrogenated amorphous silicon (a-Si:H) n-i-p junction around it. A spherical morphology of the solar cell functions as a nano-lens, focusing incoming light directly on the silver nanoneedle. We found that plasmonics, geometric optics, and Fresnel reflections affect the nanostructured solar cell performance, depending strongly on light incidence angle and polarization. This provides valuable insight in solar cell processes in which novel concepts such as plasmonics, elongated nanostructures, and nano-lenses are used.

References and links

1. M. A. Green, *Third Generation Photovoltaics: Ultra high Efficiency at Low Cost* (Springer-Verlag, Berlin, 2003).
2. G. Conibeer, "Third-generation photovoltaics," Mater. Today **10**(11), 42–50 (2007).
3. E. Ozbay, "Plasmonics: merging photonics and electronics at nanoscale dimensions," Science **311**(5758), 189–193 (2006).
4. S. A. Maier, M. L. Brongersma, P. G. Kik, S. Meltzer, A. A. G. Requicha, and H. A. Atwater, "Plasmonics: a route to nanoscale optical devices," Adv. Mater. (Deerfield Beach Fla.) **13**(19), 1501–1505 (2001).
5. H. A. Atwater and A. Polman, "Plasmonics for improved photovoltaic devices," Nat. Mater. **9**(3), 205–213 (2010).
6. R. A. Pala, J. White, E. Barnard, J. Liu, and M. L. Brongersma, "Design of plasmonic thin-film solar cells with broadband absorption enhancements," Adv. Mater. (Deerfield Beach Fla.) **21**(34), 3504–3509 (2009).
7. S. Pillai, K. R. Catchpole, T. Trupke, and M. A. Green, "Surface plasmon enhanced silicon solar cells," J. Appl. Phys. **101**(9), 093105 (2007).
8. D. M. Schaadt, B. Feng, and E. T. Yu, "Enhanced semiconductor optical absorption via surface plasmon excitation in metal nanoparticles," Appl. Phys. Lett. **86**(6), 063106 (2005).
9. B. P. Rand, P. Peumans, and S. R. Forrest, "Long-range absorption enhancement in organic tandem thin-film solar cells containing silver nanoclusters," J. Appl. Phys. **96**(12), 7519–7526 (2004).
10. V. E. Ferry, J. N. Munday, and H. A. Atwater, "Design considerations for plasmonic photovoltaics," Adv. Mater. (Deerfield Beach Fla.) **22**(43), 4794–4808 (2010).
11. S. Pillai, K. R. Catchpole, T. Trupke, and M. A. Green, "Surface plasmon enhanced silicon solar cells," J. Appl. Phys. **101**(9), 093105 (2007).
12. H. R. Stuart and D. G. Hall, "Island size effects in nanoparticle-enhanced photodetectors," Appl. Phys. Lett. **73**(26), 3815–3817 (1998).
13. H. R. Stuart and D. G. Hall, "Absorption enhancement in silicon-on-insulator waveguides using metal island films," Appl. Phys. Lett. **69**(16), 2327–2329 (1996).
14. O. Stenzel, A. Stendal, K. Voigtsberger, and C. von Borczyskowski, "Enhancement of the photovoltaic conversion efficiency of copper phthalocyanine thin film devices by incorporation of metal clusters," Sol. Energy Mater. Sol. Cells **37**(3-4), 337–348 (1995).
15. M. Westphalen, U. Kreibig, J. Rostalski, H. Lüth, and D. Meissner, "Metal cluster enhanced organic solar cells," Sol. Energy Mater. Sol. Cells **61**(1), 97–105 (2000).
16. Y. A. Akimov, W. S. Koh, and K. Ostrikov, "Enhancement of optical absorption in thin-film solar cells through the excitation of higher-order nanoparticle plasmon modes," Opt. Express **17**(12), 10195–10205 (2009).

17. V. E. Ferry, M. A. Verschuuren, H. B. T. Li, E. Verhagen, R. J. Walters, R. E. I. Schropp, H. A. Atwater, and A. Polman, "Light trapping in ultrathin plasmonic solar cells," Opt. Express **18**(S2 Suppl 2), A237–A245 (2010).
18. V. E. Ferry, M. A. Verschuuren, M. C. Lare, R. E. I. Schropp, H. A. Atwater, and A. Polman, "Optimized spatial correlations for broadband light trapping nanopatterns in high efficiency ultrathin film a-Si:H solar cells," Nano Lett. **11**(10), 4239–4245 (2011).
19. E. S. Barnard, R. A. Pala, and M. L. Brongersma, "Photocurrent mapping of near-field optical antenna resonances," Nat. Nanotechnol. **6**(9), 588–593 (2011).
20. J. N. Munday and H. A. Atwater, "Large integrated absorption enhancement in plasmonic solar cells by combining metallic gratings and antireflection coatings," Nano Lett. **11**(6), 2195–2201 (2011).
21. M. J. Naughton, K. Kempa, Z. F. Ren, Y. Gao, J. Rybczynski, N. Argenti, W. Gao, Y. Wang, Y. Peng, J. R. Naughton, G. McMahon, T. Paudel, Y. C. Lan, M. J. Burns, A. Shepard, M. Clary, C. Ballif, F.-J. Haug, T. Söderström, O. Cubero, and C. Eminian, "Efficient nanocoax-based solar cells," Phys. Status Solidi **4**(7), 181–183 (2010) (RRL).
22. J. Zhu, Z. Yu, G. F. Burkhard, C. M. Hsu, S. T. Connor, Y. Xu, Q. Wang, M. McGehee, S. Fan, and Y. Cui, "Optical absorption enhancement in amorphous silicon nanowire and nanocone arrays," Nano Lett. **9**(1), 279–282 (2009).
23. Y. Lu and A. Lal, "High-efficiency ordered silicon nano-conical-frustum array solar cells by self-powered parallel electron lithography," Nano Lett. **10**(11), 4651–4656 (2010).
24. J. Zhu, C. M. Hsu, Z. Yu, S. Fan, and Y. Cui, "Nanodome solar cells with efficient light management and self-cleaning," Nano Lett. **10**(6), 1979–1984 (2010).
25. Z. Fan, H. Razavi, J. W. Do, A. Moriwaki, O. Ergen, Y. L. Chueh, P. W. Leu, J. C. Ho, T. Takahashi, L. A. Reichertz, S. Neale, K. Yu, M. Wu, J. W. Ager, and A. Javey, "Three-dimensional nanopillar-array photovoltaics on low-cost and flexible substrates," Nat. Mater. **8**(8), 648–653 (2009).
26. J. Li, H. Yu, S. M. Wong, G. Zhang, X. Sun, P. G. Lo, and D. Kwong, "Si nanopillar array optimization on Si thin films for solar energy harvesting," Appl. Phys. Lett. **95**(3), 033102 (2009).
27. B. M. Kayes, H. A. Atwater, and N. S. Lewis, "Comparison of the device physics principles of planar and radial p-n junction nanorod solar cells," J. Appl. Phys. **97**(11), 114302 (2005).
28. J. M. Spurgeon, H. A. Atwater, and N. S. Lewis, "A Comparison between the behavior of nanorod array and planar Cd(Se, Te) photoelectrodes," J. Phys. Chem. C **112**(15), 6186–6193 (2008).
29. D. Kieven, T. Dittrich, A. Belaidi, J. Tornow, K. Schwarzburg, N. Allsop, and M. Lux-Steiner, "Effect of internal surface area on the performance of ZnO/In[sub 2]S[sub 3]/CuSCN solar cells with extremely thin absorber," Appl. Phys. Lett. **92**(15), 153107 (2008).
30. A. Belaidi, T. Dittrich, D. Kieven, J. Tornow, K. Schwarzburg, and M. Lux-Steiner, "Influence of the local absorber layer thickness on the performance of ZnO nanorod solar cells," Phys. Status Solidi **2**(4), 172–174 (2008) (RRL).
31. Y. Kuang, K. H. M. van der Werf, Z. S. Houweling, and R. E. I. Schropp, "Nanorod solar cell with an ultrathin a-Si:H absorber layer," Appl. Phys. Lett. **98**(11), 113111 (2011).
32. V. Sivakov, G. Andrä, A. Gawlik, A. Berger, J. Plentz, F. Falk, and S. H. Christiansen, "Silicon nanowire-based solar cells on glass: synthesis, optical Properties, and cell parameters," Nano Lett. **9**(4), 1549–1554 (2009).
33. L. Tsakalakos, J. Balch, J. Fronheiser, B. A. Korevaar, O. Sulima, and J. Rand, "Silicon nanowire solar cells," Appl. Phys. Lett. **91**(23), 233117 (2007).
34. M. Law, L. E. Greene, J. C. Johnson, R. Saykally, and P. Yang, "Nanowire dye-sensitized solar cells," Nat. Mater. **4**(6), 455–459 (2005).
35. M. D. Kelzenberg, S. W. Boettcher, J. A. Petykiewicz, D. B. Turner-Evans, M. C. Putnam, E. L. Warren, J. M. Spurgeon, R. M. Briggs, N. S. Lewis, and H. A. Atwater, "Enhanced absorption and carrier collection in Si wire arrays for photovoltaic applications," Nat. Mater. **9**(3), 239–244 (2010).
36. B. Tian, X. Zheng, T. J. Kempa, Y. Fang, N. Yu, G. Yu, J. Huang, and C. M. Lieber, "Coaxial silicon nanowires as solar cells and nanoelectronic power sources," Nature **449**(7164), 885–889 (2007).
37. E. Garnett and P. Yang, "Light trapping in silicon nanowire solar cells," Nano Lett. **10**(3), 1082–1087 (2010).
38. R. E. I. Schropp, "Status of Cat-CVD (Hot-Wire CVD) research in Europe," Thin Solid Films **395**(1-2), 17–24 (2001).
39. L. Novotny and B. Hecht, *Principles of Nano-Optics* (Cambridge University Press, 2008).
40. R. E. I. Schropp, K. F. Feenstra, E. C. Molenbroek, H. Meiling, and J. K. Rath, "Device-quality polycrystalline and amorphous silicon films by hot-wire chemical vapour deposition," Philos. Mag. B **76**(3), 309–321 (1997).
41. M. K. van Veen, C. H. M. van der Werf, J. K. Rath, and R. E. I. Schropp, "Incorporation of amorphous and microcrystalline silicon in n–i–p solar cells," Thin Solid Films **430**(1-2), 216–219 (2003).
42. B. J. Messinger, K. U. von Raben, R. K. Chang, and P. W. Barber, "Local fields at the surface of noble-metal microspheres," Phys. Rev. B **24**(2), 649–657 (1981).
43. U. Kreibig and M. Vollmer, *Optical Properties of Metal Clusters* (Springer, Berlin, 1995).
44. E. R. Encina, E. M. Perassi, and E. A. Coronado, "Near-field enhancement of multipole plasmon resonances in Ag and Au nanowires," J. Phys. Chem. A **113**(16), 4489–4497 (2009).
45. Y. Lee, A. Alu, and J. X. J. Zhang, "Efficient apertureless scanning probes using patterned plasmonic surfaces," Opt. Express **19**(27), 25990–25999 (2011).
46. S. Berweger, J. M. Atkin, R. L. Olmon, and R. B. Raschke, "Light on the tip of a Needle: plasmonic nanofocusing for spectroscopy on the nanoscale," Phys. Chem. Lett. **3**(7), 945–952 (2012).

1. Introduction

Light management forms a crucial component in high efficiency solar cells. Textured surfaces at the front or back contact of a solar cell that cause increased light trapping yield important improvement of the over-all efficiency. A new concept of trapping light is the use of "plasmonics", the electronic response of free electrons to light interacting with metal nanostructures [1–4]. Interest in plasmonics for photovoltaics has increased considerably since about a decade and is explored from different perspectives such as enhanced scattering, local field enhancement, and wave guiding [5–13] The first experimental investigations of plasmonic enhancement for photovoltaics involved the scattering of silver nanoparticles in an organic
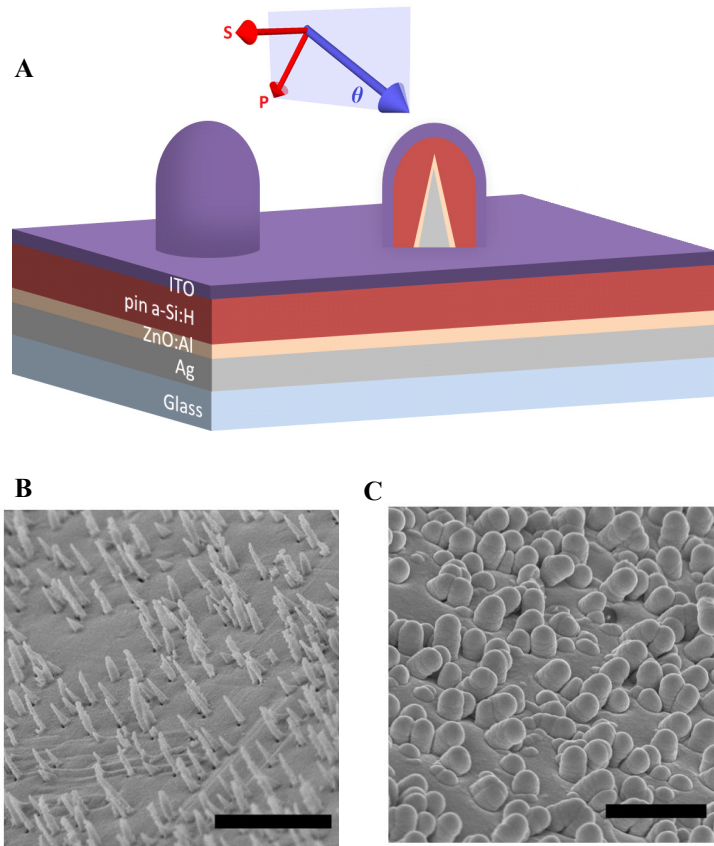

Fig. 1. (a) Schematic depiction of the nanoneedle solar cell with angle of incidence and polarization directions. The layer sequence and thickness are indicated. High resolution SEM micrographs of (b) silver nanoneedles on a silver film and (c) silver needles and film plus ZnO, n-i-p and ITO. The scale bar corresponds to 1 micrometer.

solar cell [14,15]. An absorption increase of 10-15% was found to be feasible by using such nanoparticles [16]. In nano-engineered plasmonic back reflectors that scatter strongly, light is coupled into guided modes of an ultra thin a-Si:H solar cell [17] which results in an increase of the external quantum efficiency (EQE) between 600 and 800 nm of about 8%. The spatial order of such patterned nanostructures has a strong effect on its plasmonic performance [18–20]. A recent work by Barnard et al. [21] shows the effect of plasmonic

local field enhancement underneath a silver nano-antenna on top of silicon. The measured photocurrents increased by 2.8 while the field enhancement in local "hotspots" can be significantly higher (up to 20).

Another promising approach in photovoltaics is the use of elongated nano-structured solar cells with the advantage of enhanced charge collection by short charge carrier paths and increased light absorption due to orthogonalization of light and carrier paths. This is the category of nanocoax [21], nanocone [22,23], nanodome [24], nanopillar [25,26], nanorod [27–31], and nanowire [32–37] solar cells. Employing hydrogenated amorphous silicon (a-Si:H) as light absorbing material, an efficiency of up to ~9% [18] has been reported for such nanostructured solar cells.

In this work an optical nano-antenna in the form of a silver nanoneedle is embedded in an a-Si:H solar cell. This is achieved by remarkably conformal growth using hot wire chemical vapor deposition (HWCVD) [38]. A semi-sphere on top of the nanoneedle is formed, which acts like a plano-convex lens, focusing light directly on the silver nanoneedle antenna. The pointy shape of the nano-antenna provides a wide range of plasmonic resonance conditions which satisfy excitation by light of different wavelengths, i.e. increasing the optical density. The elongated metal nanostructure potentially enables transport of surface plasmon polaritons (SPP) [39] towards the bottom of the solar cell (Fig. 1(a)). In this device the photocurrents are used to measure the effect of the nanolens combined with plasmonic nano-antenna inside the protruded solar cell. Illumination under an angle, which provides an asymmetric geometry for s- and p-polarized light, provides detailed information. S-polarized light affects the free
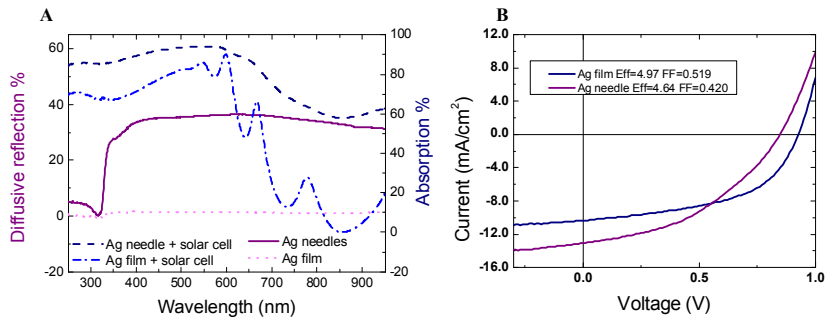

Fig. 2. (a) Left axis: diffusive reflection (scattering) of the silver nanoneedles (solid), flat silver film (dotted). Right axis: optical absorption of nanoneedles and solar cell (dashed) and flat silver film + solar cell (dashed dotted) (b) IV curves of nanoneedle and flat film solar cell under AM1.5 illumination.
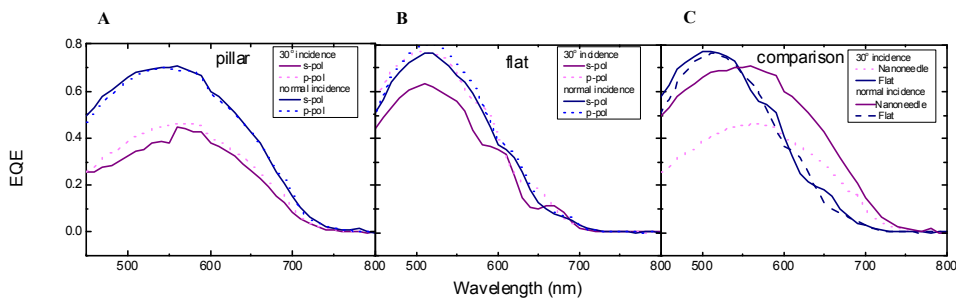

Fig. 3. EQE of (a) nanoneedle and (b) flat film solar cell at normal incidence and 30° incidence angle for s- and p-polarized light. (c) A comparison between the flat and nanoneedle solar cell

electrons in the radial direction while p-polarized light has a main resonance along the nanoneedle length. The experimental results are explained using finite-difference time-domain (FDTD) calculations, by which insight into the plasmonic and photonic properties is obtained. The main aim of this study is to obtain information about the gains and losses in these nanostructures, which do not necessarily lead to increased efficiency. However, the here obtained knowledge benefits further optimization of nanoneedle type solar cells. In this work the unique combination of plasmonics, nano-focusing, and orthogonalization in an elongated solar cell are explored.

2. Experimental section

Silver nanoneedles are formed by thermal evaporation on polycarbonate nucleopore track-etch membranes (Whatman) with a pore size of 200 nm. The polycarbonate is dissolved in chloroform after which the nanostructured silver foil was transferred on a glass substrate. During the silver deposition the pores are partially filled, resulting in the nanoneedle structure as shown in Fig. 1(b). The silver nanoneedles have a wide range of values for the length and width but are on average 650 nm high and have a base width of 90 nm. The silver film with needles is covered with a 20 nm ZnO:Al(2%) transparent conductive layer by magnetron sputtering to prevent inter diffusion with the semiconductor and optimize the reflective properties. Then, the deposition of an a-Si:H n-i-p layer stack was carried out in a multi-chamber deposition system which is described elsewhere [40] To provide conformal coverage, the intrinsic (i-) layer was deposited by HWCVD [41] using $SiH_4:H_2$ (30:60) as source gasses, whereas plasma-enhanced CVD was employed for the deposition of the p- and n-layers. $B(CH_3)_3$ and PH_3 were utilized for p- and n-doping, respectively. The n-layer, i-layer, and p-layer had a nominal thickness of 60, 400, 50 nm respectively. The arrays were sputter-coated with 2.1 mm diameter circles of transparent conducting indium tin oxide (ITO) layer with a thickness of 80 nm after the deposition of the a-Si:H n-i-p layers to provide window contacts to the cells. Each sample contained 56 solar cell dots which were all used for this experiment. High resolution scanning electron microscopy (HRSEM) imaging was performed with a Philips XL30SFEG microscope. The resulting solar cell is shown in Fig. 1(c). The current density-voltage (*J-V*) characteristics of the nanoneedle solar cells were measured using a solar simulator under one sun illumination (AM1.5G, 100 mW/cm^2) at 25°C with a Wacom dual beam solar simulator. The cell area is measured with optical microscope for calculating the current density. The EQE is measured using monochromatic light from a Xenon lamp. No DC bias light is used.

Finite-difference time-domain (FDTD) calculations were performed with commercial software (Lumerical) on a cluster super computer consisting of several hundreds of multi-core nodes. In line with the averaged nanoneedle dimensions as obtained from SEM, a silver nanoneedle of 600 nm high and 80 nm wide at the base, covered with 20 nm ZnO, 400 nm a-Si:H and 80 nm ITO was modeled. The total optical absorption is calculated by integrating the optical absorption per grid point over the entire a-Si:H structure and over the time a monochromatic light pulse resides in the structure. This leads to a time-averaged absorption. A convergency test was performed which confirmed sufficient accuracy. The calculations included 15 data points and the simulation area was 600x600x3800 nm^3. We modeled the nanoneedles as uniformly distributed using Bloch boundary conditions, which allow for an infinitely uniform distribution of needles

3. Results and discussion

To obtain a working solar cell by deposition on the pointy silver nanoneedles, the active film thickness (i-layer thickness) has to be carefully chosen. When the active layer is too thin, shunting prevents normal operation; when the active film is too thick, light will not reach the silver nanoneedle. By using HWCVD, a conformal growth of the n-i-p solar cell around the silver nanoneedle was achieved. A minimal thickness of the i-layer of 400 nm was required to

prevent shunting and still have sufficient transparency. Conformal growth of all layers is demonstrated in the HRSEM micrographs in Fig. 1(c). The silver nanoneedles are uniformly covered with the ZnO, n-i-p and ITO layers. From the cross sections of purposely broken nanoneedle solar cells the diameter after deposition was found to be about 400 nm while the height is about 1 micrometer. As the position of nanoneedles is randomly distributed the distances to each other vary. Independent of this distance, the nanoneedles were always fully covered. Patches of flat solar cell cover the area in between the nanoneedles that are further apart.

Optical scattering measurements of the bare and n-i-p covered nanoneedles show a strong effect due to the presence of nanoneedles as shown in Fig. 2(a) (left axis). The silver nanoneedles scatter much stronger than the flat silver film after the onset of the plasmon resonance wavelength (340 nm). The scattering of the silver nanoneedles has a maximum around 600 nm, which is attributed to the plasmon resonance corresponding to the specific silver nanoneedle size and shape. The absorption spectrum of the nanoneedle n-i-p a-Si:H solar cell exhibits a significant reduction in absorption intensity around 600 nm, which is caused by absorption at the a-Si:H band gap. At longer wavelengths the absorption intensity is much stronger because most of the light in the red and infra-red is not absorbed and reaches the nanoneedles. An important condition for observing a significant plasmonic effect is that the plasmon resonance energy is at or larger than the a-Si:H band gap. Only then the radiation
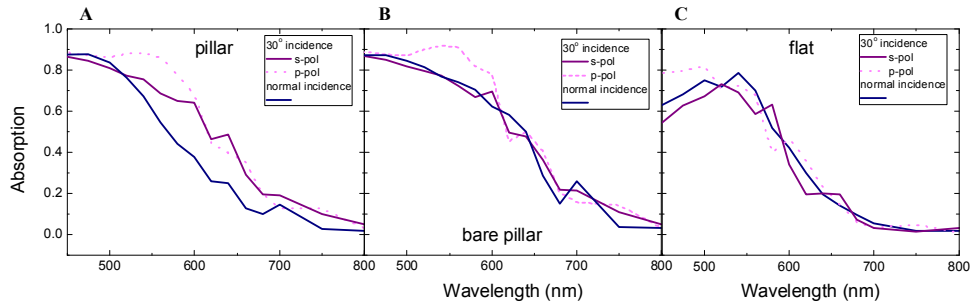

Fig. 4. Optical absorption spectra in a-Si:H (a) nanoneedle (b) without nanoneedle and (c) flat film solar cell at normal and 30° incidence for s- and p-polarized light.

absorbed or re-emitted by the nanoneedle can be detected with photocurrents. The current density-voltage (J-V) characteristics of the nanoneedle solar cells are shown in Fig. 2(b). The nanoneedle solar cells have a higher J_{SC} as compared to the flat reference while the V_{OC} values of the nanoneedle solar cells are significantly lower as a result of an increase in the defect density. The overall electrical quality of the nanoneedle solar cells as indicated by the fill factor (FF) is lower for the nanoneedle solar cells, probably caused by more shunting pathways. The energy conversion efficiencies are somewhat lower for the nanoneedle solar cells than for the flat reference solar cells taking into account the inaccuracy of 10% due to unavoidable error margins in the calibration of the simulator and the solar cell active areas. The effectiveness of the silver nanoneedles under illumination depends strongly on light absorption within a-Si:H. At low wavelengths most light will be absorbed near the upper silicon surface of the nanoneedle solar cell, not reaching the silver nanoneedle, which renders it inactive. At the large wavelengths most light passes undisturbed by a-Si:H, which makes the detection of the nanoneedle interaction with light immeasurable. Therefore, only between those spectral ranges in the window between about 550 and 670 nm a measurable effect of the nanoneedle will be possible.

To investigate the effect of the plasmonic properties of the silver nanoneedles on the surrounding solar cell, s- and p-polarized light are used to excite different plasmon resonance

modes in the nanoneedle (as shown in Fig. 1(a)). Each mode is related to a particular dimension (length or width) which can be considered a Fabry-Perot resonator. The plasmon resonance modes for s- polarized light is radial while for p-polarized light they have a strong component along the nanoneedle length. In Fig. 3 the experimental spectral response of the silver nanoneedle and flat solar cell is shown for s- and p-polarized light at normal incidence and under an incidence angle of 30°. For normal incidence the spectral response profile on the Ag nanoneedle and the flat solar cells does not depend on the polarization of light (blue curve in Fig. 3(a) and 3(b)) due to symmetry. The flat solar cell has two shoulders at 560 and 610 nm, which can be explained by constructive interference. This is not present in the nanoneedle solar cell because the large thickness variation caused by the wide range of incidence angles with respect to the solar cell surface, obscures such spectral features. The EQE of the flat cell (Fig. 3(c)) is slightly higher than that of the nanoneedle cell between 450 and 500 also due to constructive interference. Constructive interference is much more possible in the flat cell as compared to the rough nanoneedle cell in which very little flat surface is present.

The spectral response curves of the nanoneedle and flat reference solar cells taken at an incidence angle of 30° depend strongly on the polarization of light. The dependence of EQE on light polarization of the flat reference solar cells is explained by the Fresnel reflection and Brewster angle (62° for air to ITO), which results in a reflection coefficient of s-polarized light of about 0.3 while it is close to 0 for p-polarized light. This results in different light transmission for different polarizations at the solar cell surface leading to the observed difference in EQE. The flat solar cell has a higher EQE value for s-polarized light as compared to p-polarized light at 600 and 670 nm. Because of the stronger transmission for s-polarized light due to Fresnel reflection this light interferes constructively. The absorption spectrum of the flat solar cell as calculated by FDTD (Fig. 4(b)) confirms this polarization dependence at 30° incidence. At the higher wavelengths s- and p-polarized absorption spectra have optima at alternating wavelength positions due to constructive interference.
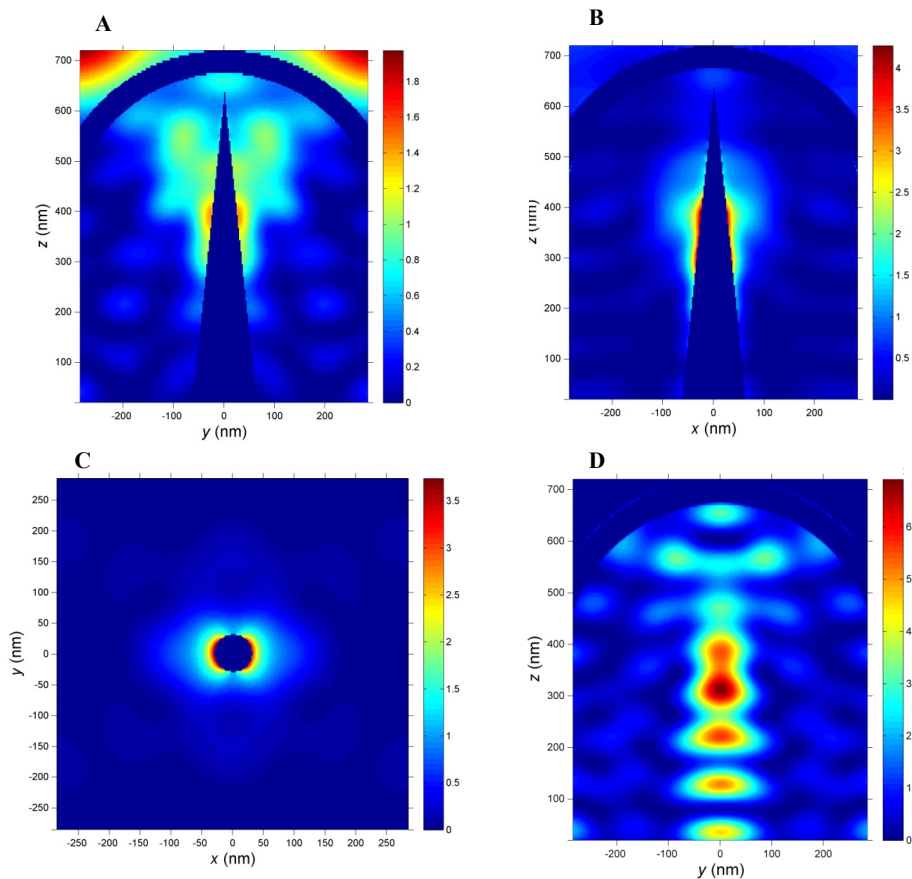
Fig. 5. Cross sections of the time-integrated photo-absorption in the a-Si:H part of the nanoneedle solar cell at 580 nm with nanoneedle (a) view perpendicular to plane of incidence (b) along plane of incidence (c) top view at z = 340 nm. Without silver nanoneedle inside, view perpendicular to plane of incidence (d) The intensity scale bar units are absorption 10^{19} m^{-3}.

At 30° incidence angle on the nanoneedle solar cell the blue and red part of the EQE spectrum are not significantly different between the two polarizations. The smaller EQE values of the nanoneedle solar cell for s-polarized light between 460 and 570 nm must be related to the presence of the silver nanoneedle. In Fig. 4(a) the FDTD calculations confirm that s-polarized light at 30° incidence is much less absorbed than p-polarized light between 500 and 600 nm while at other wavelengths the absorption is comparable. A slight shift of the position of this gap of about 30 nm is explained by a slight mismatch between the average nanoneedle size in the experiment and calculation. Because this lower absorption for s-polarized light is also present in the bare solar cell (without nanoneedle, Fig. 4(b)), the morphology in combination with Fresnel reflection is the most likely cause.

In Fig. 3(a) the EQE maximum at normal incidence is positioned approximately 26 nm blue-shifted as compared to that at 30° incidence. This indicates that relatively less light is absorbed in the red at normal incidence due to a loss mechanism. To clarify this loss, the optical absorption in the a-Si:H layer of a nanoneedle solar cell was calculated with FDTD as a function of wavelength for s- and p-polarization at normal and 30° incidence for a nanoneedle solar cell (Fig. 4(a)). In agreement with the experimental blue shift at normal incidence the FDTD nanoneedle solar cell has considerably lower absorption in the red as

compared to 30° incidence. A likely mechanism is Ohmic loss by which the moving free electrons in the metal result in the dissipation of electromagnetic energy into heat [42]. This is confirmed by comparing the FDTD calculated optical absorption of the nanoneedle solar cell with and without silver nanoneedle inside. The optical absorption slope in Fig. 4(a) at normal incidence is positioned 75 nm to the blue for the nanoneedle solar cell as compared to the bare solar cell in Fig. 4(b). This can only be explained by the nanoneedle presence leading to losses in the red part of the spectrum. The EQE difference at the short wavelengths between experiment (Fig. 3) with low EQE and FDTD calculations (Fig. 4) with strong absorption is explained by optical losses in the p-layer were most of the short wavelength light is absorbed. In the p-layer the surface defects form recombination centers, which was not included in the calculations.

The cross sections of the light absorption in the a-Si:H with and without the nanoneedle are shown in Fig. 5. The wavelength of 580 nm is chosen as it allows a full pass through the entire active layer. Pockets of high absorption are clearly distinguishable within the solar cell. Side and top view cross sections at normal and 30° incidence show that most of the light is absorbed in the central region of the nanostructured solar cell. Comparison of the side cross sections with (Fig. 5(a) and 5(b)) and without (Fig. 5(d)) nanoneedle shows clearly that the light is focused onto the nanoneedle.

The distance between high absorption spots in the cross sections is about 100 nm. Since the wavelength of 580 nm light inside the a-Si:H medium is 164 nm a constructive interference pattern has a periodicity of half that wavelength: 82 nm. Therefore these strong absorption spots are the result of constructive interference caused by the incident light interacting with its own reflections and scattering. A top view cross sections at 340 nm (Fig. 5(c)) shows that the nanoneedle forms a dipole scattering profile. This demonstrates the plasmonic response of the nanoneedles, resulting in far field scattering. This affects overall light absorption. At 30° incidence the focal point is not positioned at the nanoneedle, therefore the light-plasmon interaction is much weaker.

The nanoneedle has a small radius at the top and a large radius at the base resulting in different responses to incoming electromagnetic fields. At the silver nanoneedle tip the size is so small that visible light fully penetrates until about 27 nm [42] (the quasi-static regime). For silver particles of comparable size, about 30% of the incident energy is absorbed and lost as heat [43]. At the lower part of the nanoneedle the radius is too large for light to cross, instead retardation effects become important. A wide range of plasma resonance wavelengths are possible as shown by calculations on nanorods [44]. Although no significant effect is observed here, energy transport via SPPs to the bottom of the solar cell is in principle possible [39, 45]. How far a plasmon is able to travel is determined by the sharpness of the nanoneedle [46].

4. Conclusions

Concluding, an a-Si:H solar cell was conformally grown around a silver nanoneedle providing a unique device to measure plasmonic activity. The spherical top of the solar cell provided a unique nano-lens, focusing polarized light on the silver nanoneedle. The EQE for s- and p-polarized light at normal incidence and under an angle of 30° shows that the nanoneedle solar cell has a lower absorption for red light at normal incidence. This is confirmed by FDTD calculations. The electromagnetic field is captured by the silver nanoneedle which functions as a antenna and via the motion of free electrons (plasmons) converted into heat. Differences in EQE as a function of polarization are attributed to the nanostructured morphology in combination with Fresnel reflections. Although the efficiency did not yet improve with respect to the reference, this study provides valuable information about the interaction of the nanoneedle plasmons and cell morphology with light. This will assist the optimization of nanoneedle type solar cells. For example the aspect ratio, length and width of the nanoneedle can be further optimized. This work demonstrates that even in an

optimized geometry, where light is directly focused on a nanoneedle, the combination of plasmonics and geometrical optics needs to be finely tuned to obtain solar cell efficiency gain.

Acknowledgments